Available online at www.sciencedirect.com
ScienceDirect
Journal of Crystal Growth 310 (2008) 2353–2358
JOURNAL OF CRYSTAL GROWTH
www.elsevier.com/locate/jcrysgro

InGaAs/GaAs 3D architecture formation by strain-induced self-rolling with lithographically defined rectangular stripe arrays

I.S. Chun[b], V.B. Verma[a], V.C. Elarde[a], S.W. Kim[b], J.M. Zuo[b], J.J. Coleman[a,b], X. Li[a,b,*]

[a]*Department of Electrical and Computer Engineering, University of Illinois, Urbana, IL 61801, USA*
[b]*Department of Materials Science and Engineering, University of Illinois, Urbana, IL 61801, USA*

Available online 17 November 2007

Abstract

Three-dimensional (3D) compound semiconductor architectures can be formed when strained semiconductor layers are released from the substrate by selective etching. These 3D nanostructures have potential applications in nanoelectronics, nanophotonics and nanomechanics. In this paper, we report on the formation of $In_{0.2}Ga_{0.8}As$/GaAs 3D structures using lithographically defined micron-size, open-ended rectangular stripe patterns on films grown by metalorganic chemical vapor deposition (MOCVD). The formation process of nanotubes with diameters smaller than theoretical values has been analyzed. Unambiguous strain direction and crystallographic orientation dependence have been demonstrated. A geometry effect with respect to the longer and shorter sides of the rectangular pattern has been observed, indicating a pathway for high-degree control over the number of turns for such tubes and their positioning by lithographically defined stripe arrays.

PACS: 81.07.De; 81.05.Ea; 81.15.Gh

Keywords: A1. Nanostructure; A3. Metalorganic chemical vapor deposition (MOCVD); B2. Semiconducting III–V materials; B2. Semiconducting gallium arsenide

1. Introduction

III–V compound semiconductor nanotubes (SNTs) were first fabricated by Prinz et al. [1] in 2000, using strain-induced self-rolling of semiconductor bilayers grown by molecular beam epitaxy (MBE). They represent a new class of building blocks for nanotechnology, analogous to quantum dots, wires or wells.

The basic concept of the rolling mechanism of a SNT is illustrated in Fig. 1. For a layer with lattice constants larger than the substrate, e.g. the $In_xGa_{1-x}As$ layer on GaAs substrate in Fig. 1a, it is compressively strained when pseudomorphically deposited on the substrate (Fig. 1b). When the sacrificial layer (e.g. $Al_xGa_{1-x}As$) is selectively etched away, the strained bilayer that consists of GaAs and $In_xGa_{1-x}As$ becomes detached from the substrate (Fig. 1c). The compressively strained $In_xGa_{1-x}As$ layer deforms to expand with force F2 as labeled in Fig. 1c, while the GaAs layer on top resists the expansion with force F1. This results in a momentum, which drives the rolling action to form a tube in order to accommodate the relative strain within the GaAs/$In_xGa_{1-x}As$ bilayer. There are two essential components in such strain-induced self-rolling structures: (a) a sacrificial layer that can be selectively etched off from the substrate and the layers above it; and (b) a bilayer (two different materials or single material with two regions of different strains [2]) above the sacrificial layer that has a greater than zero net strain. The strained bilayer is the moving part that is powered by strain release. The diameter of the rolled-up tube or scroll is determined by the built-in strain and the total thickness of the bilayer, and has been modeled using a macroscopic continuous mechanical model with consistent experimental results [3–6]. Depending on the extent of undercutting, multiple numbers of rolls can be formed.

Nanotubes with inner diameters as small as 3 nm have been formed from ultra-thin InGaAs–GaAs films [1,6].

*Corresponding author. Tel.: +1 217 265 6354; fax: +1 217 244 6375.
E-mail address: xiuling@uiuc.edu (X. Li).

0022-0248/$ - see front matter © 2007 Elsevier B.V. All rights reserved.
doi:10.1016/j.jcrysgro.2007.11.044

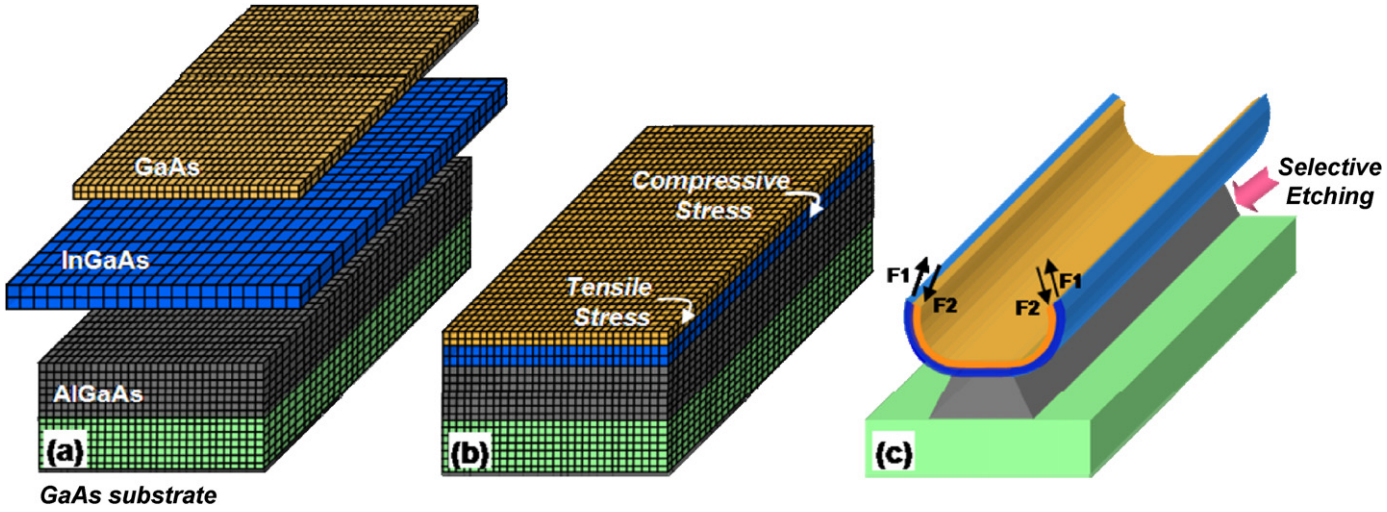

Fig. 1. Illustration of the formation mechanism of strain-induced self-rolling of a semiconductor nanotube from a rectangle stripe, illustrated with $In_xGa_{1-x}As$-GaAs bilayer and $Al_xGa_{1-x}As$ sacrificial layer.

The strain-induced formation mechanism has also been generalized to form various other kinds of three-dimensional (3D) architectures [7–9]. Self-assembled monolayers have been deposited on the bilayer to form radial superlattices [10]. 2D electron gas transport properties on cylindrical surfaces in InGaAs/GaAs rolled-up tubes have been studied [6,11,12]. Structural, optical, and electrical characterizations have been performed [13–18]. Potential applications have been proposed and some preliminary results have been demonstrated, including as micro or nanoscale building blocks for MEMS and NEMS, for microinjections and ink-jet printing [19], magnetic conductors using ferromagnetic material filled coils [20], X-ray waveguiding [13], fluidics [21], and biology [22].

It is important, for various applications, to have tubes with precisely tailored inner diameter, perfectly controlled length, desired number of turns, and pre-determined separations between individual tubes. We report here on the strain-induced self-rolling behavior of InGaAs/GaAs using lithographically defined micron-size stripe patterns. The arrays of stripes with different dimensions and orientations have allowed us to demonstrate in detail how the stripes roll into a tube or scroll, upward or downward, and left or right handed, as a function of the stripe orientation, width, length, and net strain direction of the bilayer. Our results not only verify and clarify the understanding of the strain-induced rolling process of compound semiconductor structures, but also provide further guidance on the design of 3D nano-objects for various applications.

2. Experimental procedure

Two epitaxial structures grown by metalorganic chemical vapor deposition (MOCVD) were used for the study of the strain-induced self-rolling behaviors. (1 0 0) on-axis GaAs was the growth substrate. As shown in Fig. 2, these structures consist of a strained bilayer with $In_{0.2}Ga_{0.8}As$ and GaAs at a nominal thickness of 6 nm each, and a 1.6-μm-thick $Al_{0.6}Ga_{0.4}As$ sacrificial layer. The unusually thick and relatively low aluminum composition $Al_xGa_{1-x}As$ sacrificial layer, although not necessary, was chosen for better control of etch rate when releasing the bilayer, and for visual clarity when rolling behavior is displayed. The growth sequence of $In_{0.2}Ga_{0.8}As$ and GaAs in the bilayer is reversed for Structures I and II. The growth was carried out using a Thomas Swan atmospheric pressure MOCVD reactor. TMGa, TMAl, TMIn, and AsH_3 were the precursors for Ga, Al, In, and As, respectively. The growth temperature for the InGaAs and GaAs bilayers was 625 °C. Structure II was grown with no cap layer and cooled down under high AsH_3 flow.

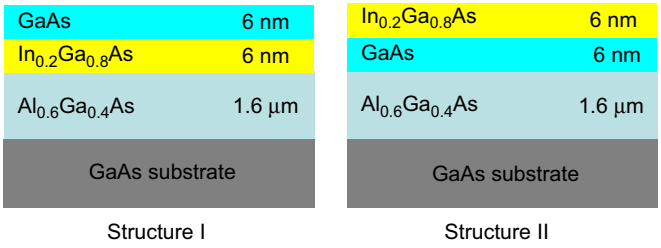

Fig. 2. The cross-sections of planar epitaxial Structures (I and II) for strain-induced tube formation. $Al_{0.6}Ga_{0.4}As$ is the sacrificial layer and the bilayer consists of $In_{0.2}Ga_{0.8}As$ and GaAs with nominal thicknesses labeled.

The mask used for photolithographic patterning contains squares and rectangles with width and length ranging from 1 to 10 μm. The fabrication of the nanotubes/scrolls was carried out using two methods. The first method involves the following steps: SiO_2 deposition, photolithographic patterning, freon-reactive ion etching to transfer the pattern to the SiO_2 layer, and inductively coupled plasma etching to transfer the pattern to the epitaxial structure down to the sacrificial $Al_{0.6}Ga_{0.4}As$ layer. In the second method, photolithographic patterning was done

directly on the epitaxial structure and wet chemical etching (H_2SO_4:H_2O_2:H_2O = 1:8:80) was used to transfer the pattern. Once the patterns were defined and all four sides of the sacrificial layer were exposed, a timed etch using 1:5 HF:H_2O was used to laterally remove $Al_{0.6}Ga_{0.4}As$ and release the bilayer from the substrate for rolling. Both methods work for the feature sizes and structures studied for this paper, but the first method is preferred for smaller feature sizes. Care has been taken to ensure that the PR is removed and does not inhibit the etching of $Al_xGa_{1-x}As$. Please note, the ragged edge appearance is a result of imperfect photoexposure during patterning. Scanning electron microscopy (SEM) imaging was used to examine the topography and diameter of the formed tubes. Cross-sectional scanning transmission electron microscopy (STEM) and energy dispersive spectroscopy (EDS) were used to measure the thickness and composition of the epitaxial planar bilayer, respectively.

3. Results and discussion

3.1. Nanotube formation process from lithographically defined micron-size rectangular stripes

The first structure examined is Structure I in Fig. 2 where GaAs is on top and the compressively strained $In_{0.2}Ga_{0.8}As$ is underneath. According to the mechanism illustrated in Fig. 1, the bilayer should roll upward when released from the substrate. Fig. 3 displays a series of SEM images showing the shape evolution of a patterned stripe as the sacrificial layer is removed selectively. This particular stripe dimension is 5 μm × 10 μm, oriented along the [0 0 1] direction. All other stripes ranging from 1 to 10 μm in width showed the same behavior. When the bilayer begins to be released from the substrate, all four edges start to roll up in the [0 0 1] and [0 1 0] directions (Fig. 3a). As the selective etching proceeds and more of the bilayer is set free, the upward rolling continues for the longer edges, while the shorter edges flatten to allow room for the upward curvature of the longer edge (Fig. 3b). Further undercutting leads to the complete rolling of the longer edge and a tube is formed, as shown in Fig. 3c.

Fig. 4 shows the STEM cross-sectional image of the epitaxial planar structure after the sample was exposed to air for nearly 4 months. The layer thicknesses of the bilayer are 5.8 and 5.2 nm for $In_{0.2}Ga_{0.8}As$ and GaAs, respectively, with ~1.2 nm native oxide on top. The indium composition in $In_{0.2}Ga_{0.8}As$ layer has been verified by EDS from the STEM sample.

The diameter of a typical tube is measured to be 884 nm, with a few nm scattering. Based on classical elasticity model, the diameter D for a tubular structure can be estimated by the following equation [4,23]:

$$D = \frac{d[3(1+m)^2 + (1+mn)[m^2 + mn)^{-1}]]}{3\varepsilon(1+m)^2},$$

where d is the total thickness ($d_1 + d_2$), m is the thickness ratio (d_1/d_2), n is the Young's modulus (Y_1/Y_2) ratio, and ε is the lattice mismatch ($(d_2-d_1)/d_1$) between the two layers. Numerical values for the parameters used are $Y_1(In_{0.2}Ga_{0.8}As) = 75.1$ and $Y_2(GaAs) = 85.6$ GPa [6], and $\varepsilon = 0.01434$. With the $In_{0.2}Ga_{0.8}As$ layer thickness fixed (5.8 nm based on STEM), the closest fit to the experimental value requires the GaAs layer thickness to be 2.8 nm, which is clearly not supported by the STEM image (Fig. 4). If we ignore the native oxide thickness and use

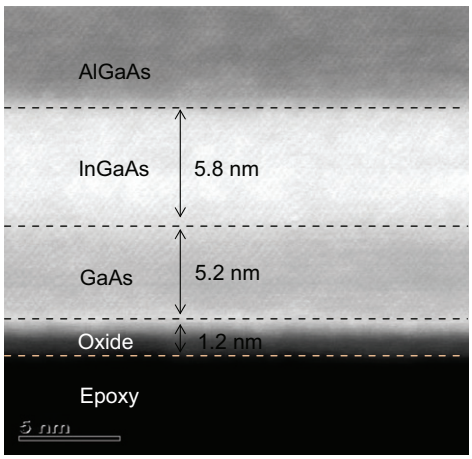

Fig. 4. High-resolution STEM image of the $In_{0.2}Ga_{0.8}As$–GaAs bilayer region for Structure I, obtained using JEOL 2010F STEM.

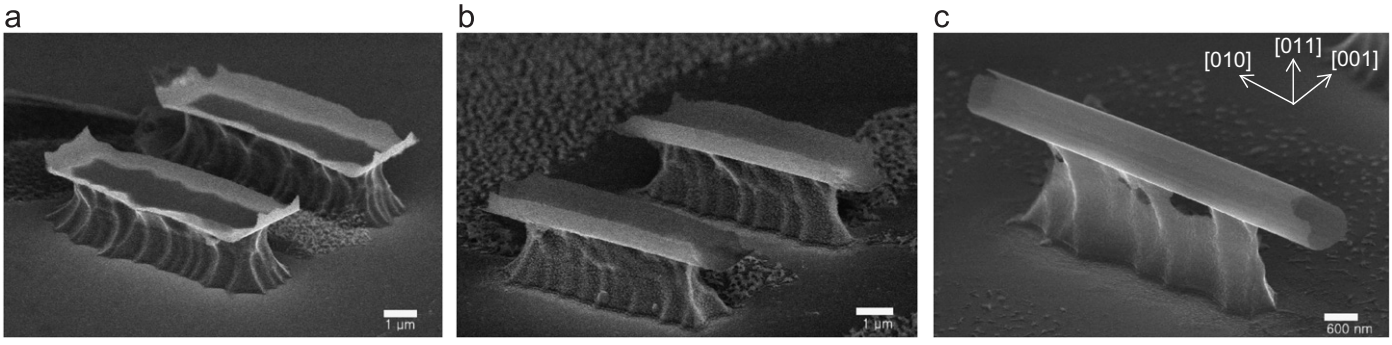

Fig. 3. SEM images of the nanotube formation process from rectangular stripes: (a) initial stage where all four sides rolling up; (b) as etching proceeds, shorter sides flatten and longer ones continue to roll and (c) the completion of rolling. The longer edge of the rectangle is oriented in the [0 1 0] direction. The tube diameter is measured to be 884 nm.

5.2 nm as the GaAs thickness as indicated by STEM, a calculated diameter of 1024 nm is obtained. The assumption here is obviously that aging (4 months) does not increase the oxide thickness (i.e. consume GaAs) further and the oxide has all been removed when the tubes were made. Therefore, at a minimum, the equation above overestimates the diameter by ~14% (1024 vs. 884 nm). A more reasonable estimate is to assume that half of the native oxide thickness (~2 ML) in the STEM sample is the consumed GaAs, i.e. the GaAs thickness was 5.8 nm when the sample was used to make the tube. The tube diameter would then be 1079 nm, which is 18% larger than the experimental value. Although some previous reports [5,24–26] did show the same trend in deviation from the predicted values, especially for ultra-thin films [27], most reports on tube sizes similar to this study demonstrated adequate fitting. This implies that additional strain or surface tension may have contributed to the rolling of the rectangular open-ended stripes with relatively low aspect ratio in the range of 1–10 in this study. In a previous report on similar tubes formed by a scratch and etch method [28], X-ray microdiffraction analysis on individual tubes has indicated only partial relaxation of the rolled up $In_xGa_{1-x}As$ layer. It can be contemplated that the relaxation extent of the $In_{0.2}Ga_{0.8}As$ layer for the mesa geometry in this study is even less due to stronger moment of torsion, which results in additional strain and a reduction of the tube diameter. Further characterization of individual tubes including TEM and spatially resolved optical studies is needed and will be reported separately.

It is also important to point out that more considerations need to be taken when predicting the tube formation from more complex structures for certain device applications. For example, a tubular optical resonator structure needs to incorporate quantum well, barrier and cladding layers together with the strained bilayer. The additional thickness from multiple layers naturally increases the tube diameter. However, the additional strain present in the quantum well or barrier layers and its distribution may require more complex models than the simple classical elasticity model.

3.2. Formation of other 3D architectures—strain and crystal orientation dependence

Using the same mask, we have photolithographically defined an array of stripe patterns identical to the ones in Fig. 3, except that the stripes are orientated along the $\langle 1\,1\,0\rangle$ direction—parallel to the major orientation flat of the substrate wafer. Using the same etching procedure to remove the sacrificial layer, we have found that the rolling occurs from the rectangle corners $\langle 1\,0\,0\rangle$, instead of the edges $\langle 1\,1\,0\rangle$, which leads to the formation of flower pedal-like, instead of tubular shapes, as shown in Fig. 5. Continued etching and rolling result in coil formation. Cubic crystals show anisotropy in elasticity, photoelasticity and certain other properties not observed in refractive index and conductivity. For GaAs, the Young's modulus in the $\langle 1\,0\,0\rangle$ direction is 85.3 GPa while it is 121.3 GPa in the $\langle 1\,1\,0\rangle$ direction [29,30]. The persistence of rolling along the $\langle 1\,0\,0\rangle$ direction, no matter how the rectangle stripes are oriented, apparently results from the anisotropy of stiffness in the cubic GaAs crystal, consistent with previous reports on GaAs and other cubic crystals [5,31,32].

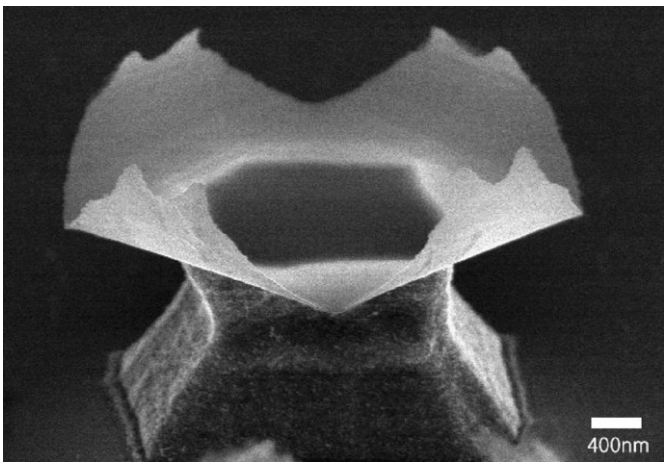

Fig. 5. A SEM image of a flower pedal-like shape from a stripe orientated in the $\langle 0\,1\,1\rangle$ direction, in contrast to the tubular shapes formed when oriented in the $\langle 0\,1\,0\rangle$ direction as in Fig. 3.

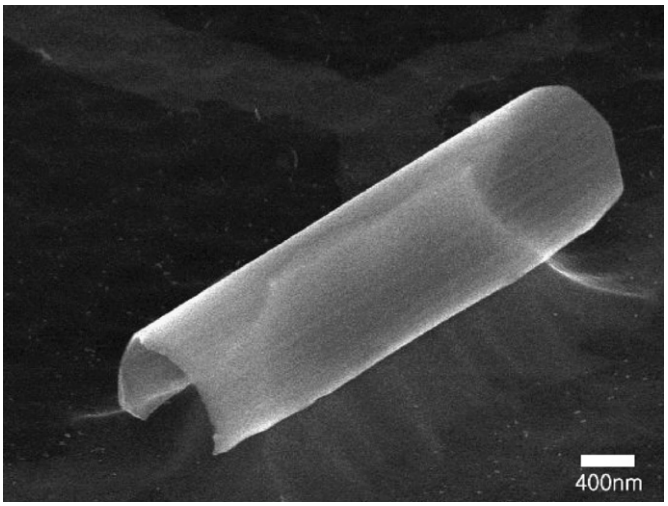

Fig. 6. A SEM image of inverted rolling of Structure II, where $In_{0.2}Ga_{0.8}As$ is placed on top of GaAs.

It can be inferred from the strain-induced self-rolling mechanism illustrated in Fig. 1, that if the strain direction is reversed, e.g. when the compressively strained layer is placed on top of the tensile strained one in the planar structure, the rolling direction should go downward. Inverted rolling has been demonstrated for semiconductor tubes made of strained Si [2] or SiGe. This is observed in Structure II where the $In_{0.2}Ga_{0.8}As$ sits on the top and GaAs on the bottom of the bilayer, as shown in Fig. 6. The demonstration of inverted $In_xGa_{1-x}As$-GaAs tubes is important for tubes with active structures such as quantum wells. In contrast to growing the active structure on top of

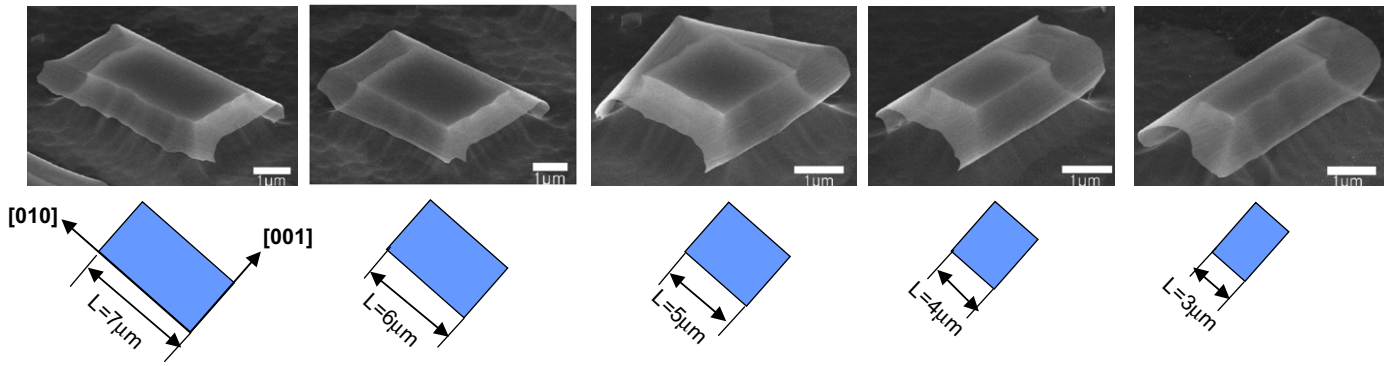

Fig. 7. SEM images of an array of inverted-rolling rectangular stripe patterns that are partially released from the substrate, demonstrating stripe orientation with respect to the width and length ratio. The widths of all the patterns are the same (5 μm) and lengths (L) vary from 3 to 7 μm, as labeled below the images.

a strained $In_xGa_{1-x}As$ layer, an entire device structure can be grown free of strain before the deposition of the strained rolling-enabling $In_xGa_{1-x}As$ layer.

3.3. Geometry effect in the formation of tubes

In previous reports, the position, length and orientation of the tubes on the substrate were predetermined by initial narrow slits fabricated using either electron, focused ion beam or crack-assisted lithography. Multiple turns were formed with prolonged etching. Barrier bars had to be used to control the outside diameter of the tubes by stopping the scrolling process in the surface region squeezed between the initial slit and stopping bar [1]. As will be demonstrated below, the geometry effect we observed from lithographically defined stripe patterns potentially allows controlled fabrication of single turn tubes.

Fig. 7 shows the rolling behavior of an array of rectangle stripe patterns with one side being 5 μm in length and the other side varied from 1 to 10 μm (only 3–7 μm are shown in the graph). Even though the orientation of [0 0 1] and [0 1 0] are equivalent in crystallography, the rolling occurs in the [0 0 1] for some and [0 1 0] for others. By examining the geometry of the stripe patterns, it becomes clear that the ratio of length to width of the rectangle stripes dictates the rolling direction in this case. The longer edges are always the moving parts, probably as a result of larger momentum compared to the shorter edges. When the pattern is square (length = width = 5 μm), the rolling seems to lose its directionality and rolling with all sides or in a random direction seems to occur. Such geometry dependence has been observed for both Structure I (upward rolling) and II (downward rolling). This phenomenon enables the formation of single turn tubes by designing the shorter edge of the rectangular mesa to match the tube circumference.

4. Conclusion

An array of stripe patterns with dimensions of 1–10 μm on either side, defined by photolithography, dry or wet chemical etching, have been used to fabricate strain-induced self-rolling 3D structures. The formation of $In_{0.2}GaAs/GaAs$ architectures of tubular and flower–pedal-like shapes both upward and downward relative to the substrate surface have been demonstrated. It has been clearly shown that strain driven rolling initiates preferably in ⟨0 1 0⟩ crystallographic orientation rather than ⟨1 1 0⟩ for the (1 0 0) GaAs surface. The geometry effect where rolling of the longer edges overtakes that of the short ones provides a method to fabricate tubes with precisely a single turn or pre-determined number of turns of the designed diameter. The diameter is smaller than what is expected from the classical elastic model for these micron-size open-ended rectangular stripe patterns with low aspect ratio. More investigation is needed to uncover additional strain involved in the rolling mechanism.

Acknowledgments

X. Li acknowledges her startup fund from the University of Illinois. TEM work was supported by the US Department of Energy Grant DEFG02-01ER45923, and carried out at the Center for Microanalysis of Materials at the Frederick Seitz Materials Research Laboratory, which is partially supported by the US Department of Energy under Grant DEFG02-91-ER45439.

References

[1] V.Y. Prinz, V.A. Seleznev, A.K. Gutakovsky, A.V. Chehovskiy, V.V. Preobrazhenskii, M.A. Putyato, T.A. Gavrilova, Physica E (Netherlands) 6 (2000) 828.
[2] R. Songmuang, Ch. Deneke, O.G. Schmidt, Appl. Phys. Lett. 89 (2006) 223109.
[3] C. Deneke, C. Muller, O.G. Schmidt, Mater. Res. Soc. Symp. Proc. 728 (2002) 141.
[4] P.O. Vaccaro, K. Kubota, T. Aida, Appl. Phys. Lett. 78 (2001) 2852.
[5] L. Zhang, S.V. Golod, E. Deckardt, V. Prinz, D. Grutzmacher, Physica E (Netherlands) 23 (2004) 280.
[6] O.G. Schmidt, C. Deneke, S. Kiravittaya, R. Songmuang, H. Heidemeyer, Y. Nakamura, R. Zapf-Gottwick, C. Muller,

N.Y. Jin-Phillipp, IEEE J. Sel. Top. Quantum Electron. 8 (2002) 1025.
[7] H. Paetzelt, V. Gottschalch, J. Bauer, H. Herrnberger, G. Wagner, Phys. Stat. Sol. (A)—Appl. Res. 203 (2006) 817.
[8] M. Mason, T. Yeoh, Z. Feinberg, M. Leung, M. Tasci, V.C. Elarde, J.J. Coleman, Mater. Res. Soc. Symp. Proc. 924 (2006) Z06.
[9] L. Zhang, E. Deckhardt, A. Weber, C. Schonenberger, D. Grutzmacher, Nanotechnology 16 (2005) 655.
[10] Ch. Deneke, U. Zschieschang, H. Klauk, O.G. Schmidt, Appl. Phys. Lett. 89 (2006) 263110.
[11] N. Shaji, H. Qin, R.H. Blick, L.J. Klein, C. Deneke, O.G. Schmidt, Appl. Phys. Lett. 90 (2007) 042101.
[12] G.J. Meyer, I. Knezevic, J. Comput. Electron. 6 (2007) 219.
[13] Ch. Deneke, O.G. Schmidt, Appl. Phys. Lett. 89 (2006) 123121.
[14] N.Y. Jin-Phillipp, J. Thomas, M. Kelsch, C. Deneke, R. Songmuang, O.G. Schmidt, Appl. Phys. Lett. 88 (2006) 33113.
[15] S. Mendach, O. Schumacher, H. Welsch, C. Heyn, W. Hansen, M. Holz, Appl. Phys. Lett. 88 (2006) 212113.
[16] K. Kubota, P.O. Vaccaro, N. Ohtani, Y. Hirose, M. Hosoda, T. Aida, Physica E (Netherlands) 13 (2002) 313.
[17] S. Mendach, R. Songmuang, S. Kiravittaya, A. Rastelli, M. Benyoucef, O.G. Schmidt, Appl. Phys. Lett. 88 (2006) 111120.
[18] N. Ohtani, K. Kishimoto, K. Kubota, S. Saravanan, Y. Sato, S. Nashima, P. Vaccaro, T. Aida, M. Hosoda, Physica E (Netherlands) 21 (2004) 732.
[19] A.V. Prinz, V. Ya. Prinz, in: Seventh International Conference on Nanometer-Scale Science and Technology and 21st European Conference on Surface Science, 2002, pp. 2.
[20] O.G. Schmidt, C. Deneke, Y.M. Manz, C. Muller, Physica E: Low-Dimensional Systems Nanostruct. 13 (2002) 969.
[21] D.J. Thurmer, C. Deneke, M. Yongfeng, O.G. Schmidt, Appl. Phys. Lett. 89 (2006) 223507.
[22] A.V. Prinz, V.Ya. Prinz, Surf. Sci. 532–535 (2003) 911.
[23] Y.C. Tsui, T.W. Clyne, Thin Solid Films 306 (1997) 52.
[24] C. Giordano, M.T. Todaro, A. Salhi, L. Martiradonna, I. Viola, A. Passabi, L. Carbone, G. Gigli, A. Passaseo, M. De Vittorio, Microelectron. Eng. 84 (2007) 1408.
[25] R. Songmuang, N.Y. Jin-Phillipp, S. Mendach, O.G. Schmidt, Appl. Phys. Lett. 88 (2006) 21913.
[26] F. Cavallo, R. Songmuang, C. Ulrich, O.G. Schmidt, Appl. Phys. Lett. 90 (2007) 193120.
[27] V.Ya. Prinz, S.V. Golod, J. Appl. Mech. Tech. Phys. 47 (2006) 867.
[28] B. Krause, Ch. Mocuta, T.H. Metzger, C. Deneke, O.G. Schmidt, Phys. Rev. Lett. 96 (2006) 165502.
[29] R.I. Cottam, G.A. Saunders, J. Phys. C (Solid State Phys.) 6 (1973) 2105.
[30] W.A. Brantley, J. Appl. Phys. 44 (1973) 534.
[31] V.Ya. Prinz, Microelectron. Eng. (Netherlands) 69 (2003) 466.
[32] S. Mendach, O. Schmacher, C. Heyn, S. Schnull, H. Welsch, W. Hansen, Physica E (Netherlands) 23 (2004) 274.